Haider Ifaz T (Orcid ID: 0000-0002-6445-7291)
Sawatsky Andrew (Orcid ID: 0000-0003-3995-4306)
Kostenuik Paul J (Orcid ID: 0000-0001-7209-1368)
Boyd Steven Kyle (Orcid ID: 0000-0002-2930-5997)
Edwards William Brent (Orcid ID: 0000-0002-3623-9764)

Twelve months of denosumab and/or alendronate is associated with improved bone fatigue life, microarchitecture, and density in ovariectomized cynomolgus monkeys

Ifaz T. Haider[1,2]
Lindsay L. Loundagin[1,2,4]
Andrew Sawatsky[1,2]
Paul J. Kostenuik[5]
Steven K. Boyd[2]
W. Brent Edwards[1,2,3*]

[1]Human Performance Lab, Faculty of Kinesiology, University of Calgary

[2]McCaig Institute for Bone and Joint Health, Cumming School of Medicine, University of Calgary

[3]Department of Biomedical Engineering, Schulich School of Engineering, University of Calgary

[4]Department of Anatomy, Physiology and Pharmacology, University of Saskatchewan

[5]Phylon Pharma Services, Newbury Park, CA, USA; and School of Dentistry, University of Michigan (Adjunct)

*Corresponding author: wbedward@ucalgary.ca

This is the author manuscript accepted for publication and has undergone full peer review but has not been through the copyediting, typesetting, pagination and proofreading process, which may lead to differences between this version and the Version of Record. Please cite this article as doi: 10.1002/jbmr.4758

Abstract

Prolonged use of antiresorptives like the bisphosphonate alendronate (ALN) and the RANKL inhibitor denosumab (DMAb) are associated with rare cases of atypical femoral fracture (AFF). The etiology of AFF is unclear, but it has been hypothesized that potent osteoclast inhibitors may reduce bone fatigue resistance. The purpose of this study was to quantify the relationship between antiresorptive treatment and fatigue life (cycles to failure) in bone from ovariectomized cynomolgus monkeys. We analyzed humeral bone from 30 animals across five treatment groups. Animals were treated for 12 months with s.c. vehicle (VEH), s.c. DMAb (25 mg/kg/month), or i.v. ALN (50 μg/kg/month). Another group received 6 months VEH followed by 6 months DMAb (VEH-DMAb), and the final group received 6 months ALN followed by 6 months DMAb (ALN-DMAb). 240 cortical beam samples were cyclically tested in 4-point bending at 80, 100, 120, or 140 MPa peak stress. High resolution imaging and density measurements were performed to evaluate bone microstructure and composition. Samples from the ALN ($p = 0.014$), ALN-DMAb ($p=0.008$), and DMAb ($p < 0.001$) groups illustrated higher fatigue-life measurements than VEH. For example, at 140 MPa the VEH group demonstrated a median ± IQR fatigue life of 1987 ± 10593 cycles, while animals in the ALN, ALN-DMAb, and DMAb groups survived 9850 ± 13648 (+395% vs. VEH), 10493 ± 16796 (+428%), and 14495 ± 49299 (+629%) cycles, respectively. All antiresorptive treatment groups demonstrated lower porosity, smaller pore size, greater pore spacing, and lower number of canals vs. VEH ($p < 0.001$). Antiresorptive treatment was also associated with greater apparent density, dry density, and ash density ($p \leq 0.03$). We did not detect detrimental changes following antiresorptive treatments that would explain their association with AFF. In contrast, 12 months of treatment may have a protective effect against fatigue fractures.

Keywords: osteoporosis, atypical femoral fracture, insufficiency fracture, antiresorptive, μCT

1.0 Introduction

Osteoporosis is a metabolic disease characterized by low bone density and quality, resulting in increased bone fragility and risk of fracture[1]. Once seen as an inevitable consequence of aging, advances in screening and treatment have helped to reduce the burden of this disease[2]. In particular, antiresorptive drugs like the bisphosphonate alendronate (ALN) and the RANKL ligand (RANKL) inhibitor denosumab (DMAb) are important mainstays of modern osteoporosis treatment. Through different mechanisms, these drugs inhibit bone loss by reducing bone resorption, which typically leads to increased bone mineral density (BMD) over time via the refilling of existing remodeling spaces and increased matrix mineralization. Consequently,

numerous studies demonstrate that these drugs increase bone density [3–8] and strength[9,10] and reduce the risk of osteoporotic fracture[6,7,11,12].

Despite the efficacy in reducing osteoporotic fracture risk, there are concerns that prolonged use of antiresorptives, including DMAb and ALN, increases the risk of rare, but serious, atypical femoral fracture (AFF). Among other features[13], these predominantly transverse fractures of the femoral shaft or subtrochanteric region occur in the absence of notable trauma and are often associated with prodromal pain and localized periosteal bone thickening, reminiscent of a fracture callus. As a result, AFFs are believed to occur from mechanical fatigue, i.e., progressive damage accumulating from repeated submaximal loading which leads to eventual material failure. The prevailing hypothesis suggests that prolonged use of antiresorptive drugs may cause bone to become more brittle with time, reducing fatigue resistance, and increasing risk of AFF [13].

Support for this mechanistic relationship between AFF and antiresorptive use has been equivocal. Though there is not yet a consensus on tissue-level changes following the use of antiresorptive agents[14], some studies show that these drugs are associated with potentially adverse changes in collagen quality [15–17], mineral heterogeneity [17,18], and microdamage accumulation [19,20]. However, beneficial changes also occur across multiple dimensional scales. These treatments are associated with higher bone density [3,4], which is likely to reduce stress and strain under loading. Antiresorptive treatment is also associated with reductions in the number and size of haversian canals[16] – changes which are associated with fatigue life improvements in *in-vitro* testing [21]. It is currently unclear how these changes interact to influence overall toughness and fatigue life. As summarized in recent reviews[14,22], results from mechanical testing studies have been inconclusive: some studies report relative reductions in toughness or

energy to failure following antiresorptive use [23–25] while others did not [16,20,23,26,27]. Only a few studies have looked at fatigue life directly[28,29] via *in-vitro* testing, and it is difficult to draw a strong conclusion due to small sample sizes and/or methodological choices[14]. None of these previous studies examined fatigue life after treatment with DMAb, which typically reduces bone resorption to a greater extent than with high doses of potent bisphosphonates[30].

The purpose of this study was to use an ovariectomized cynomolgus monkey model to quantify the relationship between 12 months of antiresorptive treatment and bone fatigue life. This non-human primate (NHP) model is commonly used in orthopaedic research [31,32]; the animals share important similarities to humans, including the fact that their cortical bone undergoes haversian remodeling [31]. Samples of cortical bone harvested from the humeral shaft were cyclically loaded to failure in a four-point bending configuration. We used micro-computed tomography (μCT) and density measurements to provide insight into the underlying mechanisms responsible for any observed differences in bone fatigue life.

2.0 Methods

2.1 Animal Model

This was a secondary use protocol, where we analyzed bone from a previous GLP (Good Laboratory Practices) study of ovariectomized cynomolgus monkeys after antiresorptive treatment[26]. Specifically, 45 NHPs were received from Mauritius Island, aged 9-14 years upon arrival. Animals were housed two per cage in an indoor AAALAC accredited facility where they were provided water *ad libitum* and fed twice daily with a certified Hi-Fiber Primate Diet (5K91 from PMI Nutrition International Inc). Ovariectomy was performed after an acclimatization period of 4-5 weeks. Animals then received 12 monthly injections of subcutaneous (s.c.) vehicle

(VEH; n=10), intravenous (i.v.) ALN (50 μg/kg, n = 10), or s.c. DMAb (25 mg/kg, n = 9). Two additional groups received 6 months of s.c. VEH followed by 6 months of s.c. DMAb (VEH-DMAb; n=7), or 6 months of i.v. ALN followed by 6 months of s.c. DMAB (ALN-DMAb; n= 9) (Figure 1a). For the current analyses, we selected a convenience sample of 30 animals, comprising 6 per group, as this was the largest number of animals allowing for a balanced representation of sample harvest sites across all load levels (detailed in section 2.2 below). Animals were sacrificed after 12-months of treatment. Femurs were harvested for histomorphometry and destructive biomechanical testing, as previously reported [33,34]; right humeri were fresh-frozen at -30°C after necropsy until their use in the current study, which was approved by the University of Calgary's Animal Care Committee.

2.2 Mechanical Fatigue Testing

Small prismatic beams of cortical bone were harvested from the proximal 1/3 (20-40% segment length, measured from proximal end) and midshaft (40-60% segment length) of the humerus (Figure 1). In the femur, the proximal and midshaft of the bone are the most common sites of AFF[35]. Samples were cut with a precision saw and subsequently polished to a nominal size of 1.5 x 1.5 x 22 mm. The length of the beam was parallel to the long axis of the bone, and particular care was taken to ensure similarity between samples, with small variance in height and width of the cross section (achieved standard deviation = 0.08 mm). At this stage, the investigative team was blinded to the specific treatment associated with each group. After preparation, samples were wrapped in tissue paper soaked with phosphate-buffered saline (PBS) and stored at -30°C prior to fatigue testing.

A material testing machine (Electropulse E3000; Instron, Norwood, MA) was used to test each sample cyclically in a 4-point bending configuration. As shown in Figure 1, the span of the outer supports was 16 mm, and the span of the inner supports was 8 mm. Tests were conducted in a temperature-controlled PBS bath at 37°C. Each sample was loaded sinusoidally at 2 Hz until rupture or a predefined runout of 1 million cycles. Samples were loaded to a peak stress of either 80, 100, 120, or 140 MPa, which was achieved by calculating a unique load for each sample based on measured cross section, using traditional engineering equations for the bending of slender beams. These loading magnitudes provided fatigue-life measurements spanning the low- to high-cycle fatigue regimen. Specifically, preliminary testing suggested that these stress levels would cause failure in 1000-1,000,000 cycles. For context, 100,000 cycles is estimated to represent approximately one month of lower-limb loading in humans[36]. The minimum cyclic stress was set at $1/10^{th}$ of the peak stress for each load level (R ratio = 0.1). A total of 240 samples (per group: 48 samples from six animals) were selected for testing, with 60 samples tested at each of the four load levels (12 samples per group for each load level). At each load level, the 12 samples per group were all obtained from the identical harvest sites and contained six samples each from the proximal and midshaft sections of the bone. Furthermore, we had three samples each from the medial, lateral, anterior, and posterior quadrants of the bone. Load levels were tested in increasing order. Within each load level, we tested all samples from 1 animal, then tested all samples from another animal from a different treatment group chosen at random; this was repeated until the load level was complete.

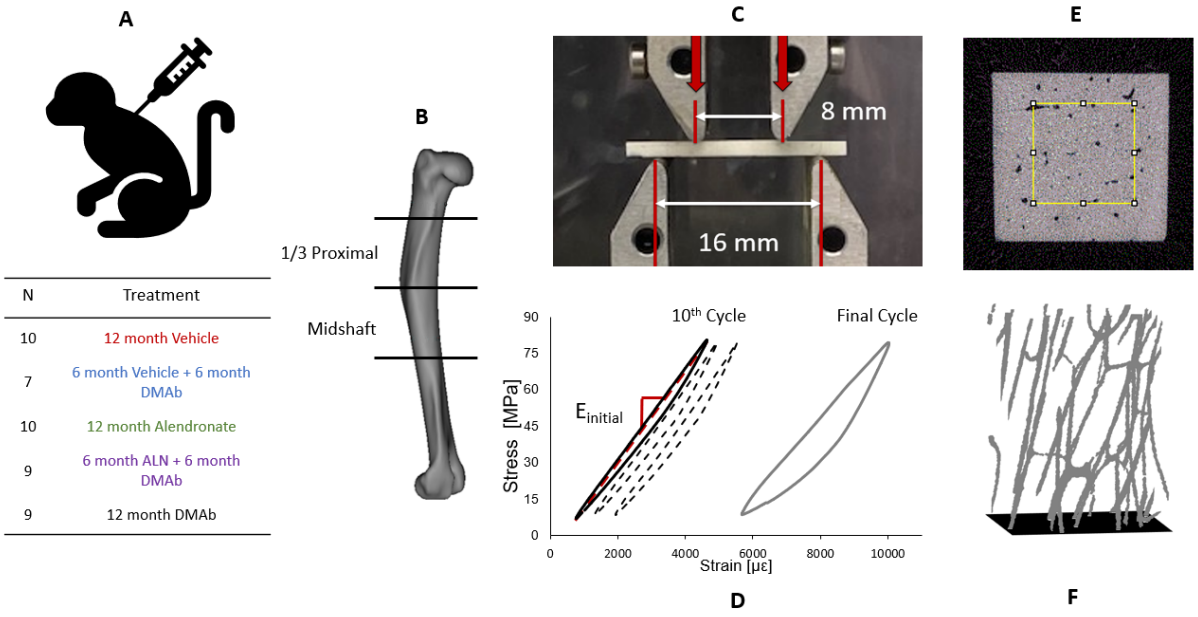

N	Treatment
10	12 month Vehicle
7	6 month Vehicle + 6 month DMAb
10	12 month Alendronate
9	6 month ALN + 6 month DMAb
9	12 month DMAb

Figure 1. Overview of mechanical testing and imaging. A: Cynomolgus monkeys were treated for 12 months with vehicle, alendronate, denosumab, or a combination thereof[26]. B: Samples were obtained from the proximal third (20-40% segment length) and midshaft (40-60% segment length) of the humerus. C: Prismatic beam samples were tested in a 4-point bending configuration with outer and inner span of 16 mm and 8 mm, respectively. D: Hysteresis data collected during cyclic loading was used to measure modulus ($E_{initial,}$; red line) and cyclic energy dissipation (area under curve, not shown). E: Samples were imaged using µCT, and a 0.75 x 0.75 x 1 mm region of interest (yellow box) was analyzed. F: Pore space was identified using an automatic algorithm implemented in MATLAB and assessed using BoneJ plugins.

In addition to recording the number of cycles to failure, we computed mechanical measures based on stress and strain during each test, measured from recorded position and force data, respectively. Secant modulus for each i^{th} cycle (E_i) was calculated from recorded stress (σ) and strain (ε) at the peak (max) and trough (min) of each loading cycle:

$$E_i = \frac{\sigma_{max,i} - \sigma_{min,i}}{\varepsilon_{max,i} - \varepsilon_{min,i}} \qquad \text{(Eq. 1)}$$

Initial modulus ($E_{initial}$) was reported as the secant modulus after 10 cycles[28], and modulus loss (E_{loss}) was reported as the ratio of secant modulus of the last loading cycle vs $E_{initial}$. Energy loss per unit volume was computed from the difference in area between the loading and unloading portion of the stress/strain curve. For this analysis, position and force data were collected at 400 Hz. Due to the long duration of some fatigue tests, we collected data intermittently at

progressively longer intervals over the test duration. The first 100 cycles were recorded fully. From cycles 100-1000 we recorded 10 of every 100 cycles, from cycles 1000-10000 we recorded 10 of every 1000 cycles, and from 10000 onward we recorded 10 of every 10000 cycles. Upon sample failure, the last 10 cycles were recorded automatically from the system buffer and were also included in this analysis. Total energy dissipation was calculated by summing energy dissipation for all cycles, using linear interpolation to estimate dissipation for cycles where the hysteresis loops were not recorded.

2.3 µCT imaging

After fatigue loading, we used high-resolution µCT imaging to quantify bone microarchitecture of each specimen. A 3 mm long section was cut from the end of each bone sample, i.e., a region of zero cyclic stress, and scanned on a Scanco µCT35 (Scanco Medical, Switzerland). Images were collected with a respective beam voltage and current of 55 kVp and 145 µA; resulting scans were reconstructed with an isotropic voxel size of 3 µm. A 0.75 x 0.75 x 1 mm region of interest was identified (Figure 1), and bone was segmented using a semi-automatic algorithm implemented in MATLAB (r2018a). First, a 3x3 median filter was used to smooth out extraneous noise. Next, bone was segmented from background via intensity-based thresholding. The threshold value for bone was identified as 60% of the mode of pixel intensities throughout the image; this value was selected by the investigators after assessing representative samples. The void space was assessed, and all interconnected void regions were identified. Regions smaller than 50 voxels were removed as they were likely remnants of image noise. Similar to previous work from our lab [37], the resulting binary images were then analyzed using BoneJ plugins[38] to calculate porosity, canal thickness, and canal spacing. Images were then skeletonized, and canal number was calculated as the number of junctions plus one.

2.4 Density measurements

After scanning, the 3 mm long samples were measured and weighed to establish specimen density. The recent cut edge of the specimen was sanded by hand to ensure a smooth rectangular section, the dimensions of which were measured with calipers to establish sample volume. The sample was then hydrated in PBS for a minimum of 24 hours before wet-weight was measured. The sample was then dried in a muffle furnace (FB1415M, Fisher Thermo Scientific) at 100 °C for 1 hour, after which the dry weight was measured. Finally, the sample was heated again at 600 °C for 12 hours, after which the ash weight was recorded [37,39]. From these measurements, we calculated apparent, dry, and ash densities for each specimen. We also reported the ratio of ash weight to dry weight as the ash fraction. Here, ash density is a measure of mineral content alone, while dry density is a measure of both mineral and organic compounds (primarily collagen). Thus, ash fraction provides insight into the relative composition of mineral vs. organic materials in the bone.

2.5 Statistical Analysis

Mechanical fatigue behavior was analyzed using a parametric survival analysis to account for the censored nature of the fatigue life data. Similar to our previous work[40], variation in observed fatigue life was described using a log-normal accelerated failure time model of the form:

$$\log\,(T) = \beta_0 + \beta_1 \cdot \log\left(\sigma_{peak}\right) + \gamma Z + [additional\ covariate\ terms] \quad \text{(Eq. 2)}$$

where T is the number of cycles to failure for a sample and σ_{peak} is the peak stress during cyclic loading. Variables β_0 and β_1 are model fit parameters. Z is a random variable following a standard normal distribution, and γ is a model-fit scale factor. For additional covariate terms, we looked at the effect of treatment group as well as an interaction between group and load level (group x stress).

A different statistical model was used to assess μCT and density data. After performing Levene's test for homogeneity of variance and Shapiro-Wilk's test for normality, these measures were all assessed using a non-parametric Kruskal-Wallis test. If a significant overall group effect was detected, pairwise comparisons between groups were performed using Dunn's procedure to correct for multiplicity. All statistical tests were assessed at a significance level of 0.05.

3.0 Results

Survival analysis revealed a significant effect of loading level ($p < 0.001$), where samples loaded at higher cyclic stress failed sooner than those at lower stress. The model also demonstrated statistically significant differences among treatment groups, but no group x stress interaction was detected ($p \geq 0.13$). Samples from animals treated with ALN ($p = 0.014$), ALN-DMAb ($p=0.008$) or DMAb ($p < 0.001$) survived more cycles than samples from animals treated with VEH at each respective loading level. For example, at the 140 MPa load level, samples from the VEH group survived a median ± IQR of 1987 ± 10593 cycles, whereas samples from the ALN, ALN-DMAb, and DMAb groups respectively survived 9850 ± 13648 (+395% difference relative to VEH), 10493 ± 16796 (+428% vs. VEH), and 14495 ± 49299 (+629% vs VEH) cycles until failure. Group differences at all other load levels are shown in greater detail in Figure 2 and Table 1; Figure 3 shows these same data plotted in a more traditional log-log curve of stress vs. fatigue life. Antiresorptive treatment was also associated with greater initial modulus ($p < 0.001$) and energy dissipation ($p=0.018$), and post-hoc analysis showed significant differences between animals treated with VEH vs DMAb ($p < 0.001$ and $p = 0.016$ for initial modulus and energy dissipation, respectively). As shown in Table 2, animals in the VEH group demonstrated values of 16.94 ± 6.60 GPa and 1.53 ± 3.16 J/mm^3 for initial modulus and energy

dissipation, respectively. In contrast, animals in the DMAb group demonstrated measures of 19.82 ± 6.22 GPa (+17% vs. VEH) and 4.40 ± 7.95 J/mm^3 (+187% vs. VEH), respectively.

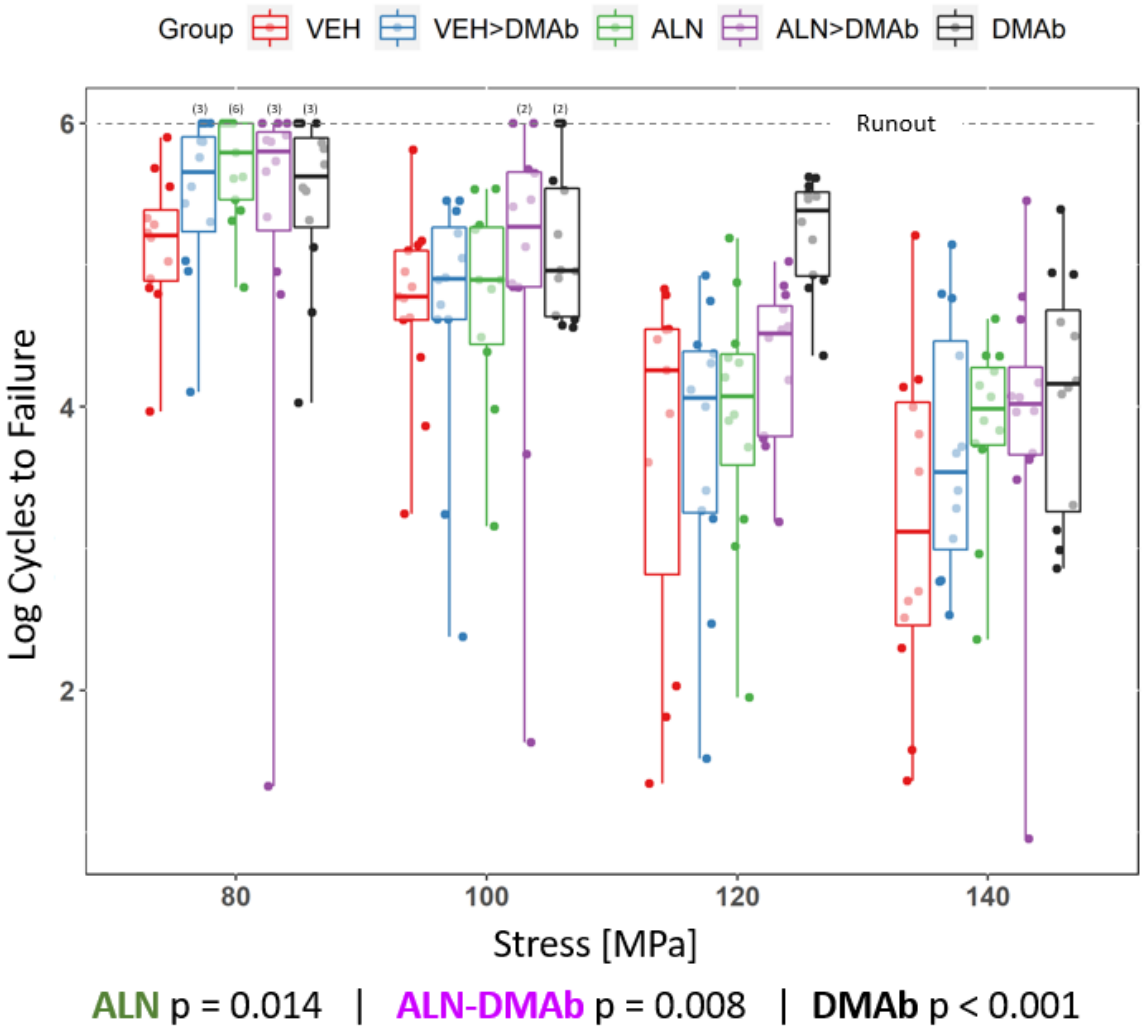

Figure 2. Results from mechanical fatigue tests. Survival analysis demonstrated a significant effect of load level ($p < 0.001$), where samples at higher loads survived fewer cycles until failure. Moreover, the analysis also demonstrated that samples from animals treated with ALN (green; $p= 0.014$) ALN-DMAb (purple; $p=0.008$) and DMAb (black; $p < 0.001$) survived more cycles than samples from animals treated with VEH. Boxes indicate the 25th, 50th, and 75th percentile of data, and whiskers indicate the full range. Bracketed numbers indicate number of samples that survived to a runout of 1 million cycles.

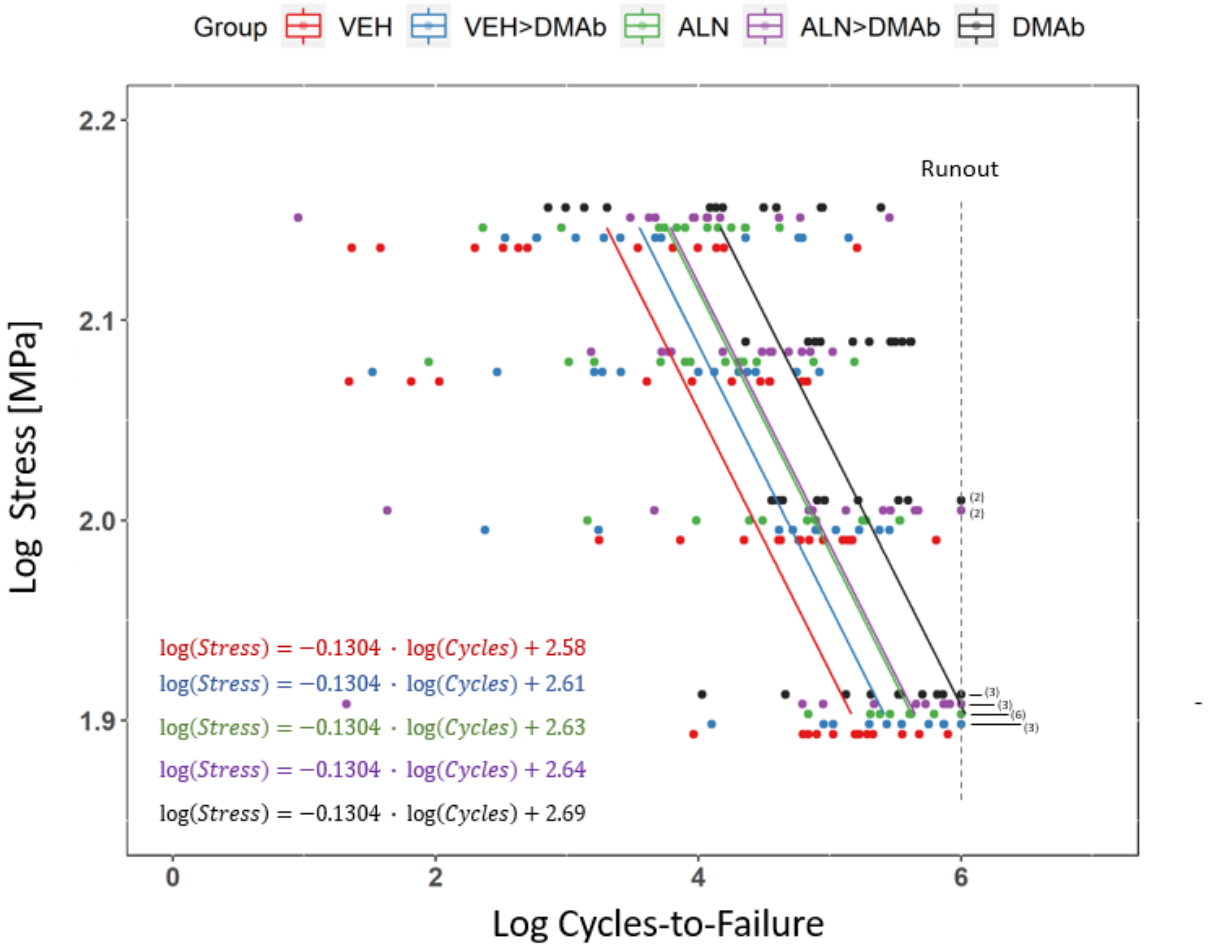

Figure 3. Stress vs. fatigue life relationships from mechanical fatigue tests. Lines indicate the stress-life relationship as predicted by our survival analysis model. These datapoints are the same as those shown in Figure 2. Bracketed numbers indicate the number of samples that survived to a runout of 1 million cycles. Group x stress interactions were not significant.

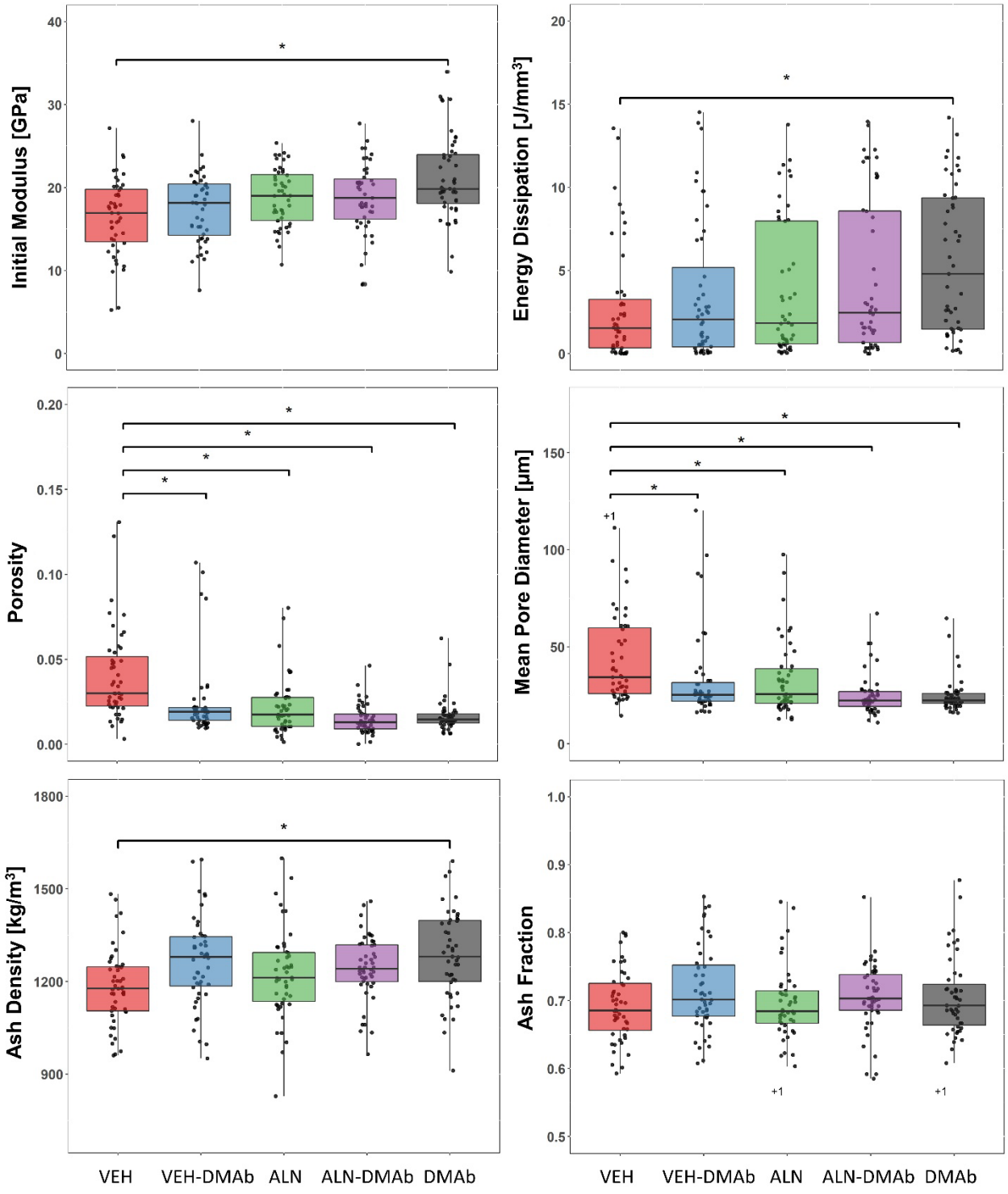

*Figure 4. Select mechanical [Top], µCT [Middle], and density measures [bottom]. All treatment groups demonstrated either beneficial differences or no significant difference vs. VEH. Beneficial differences were most numerous for the 12-month DMAb group compared to VEH, which demonstrated greater initial modulus, energy dissipation, pore diameter, and ash density, as well as lower porosity vs. VEH. *indicates $p \leq 0.05$. The "+1" symbol indicates one datapoint that is not visible on this scale.*

Differences in fatigue life and mechanical properties were accompanied by differences in μCT measures of bone microarchitecture (Kruskall-Wallis $p \leq 0.003$). Post-hoc comparisons demonstrated that, compared to VEH, all active therapy groups had lower porosity, mean pore diameter, mean pore spacing, and number of canals. For these four parameters, animals in the VEH group demonstrated mean ± SD values of 0.031 ± 0.032, 34.20 ± 34.50 μm, 242.08 ± 56.10 μm, and 24764 ± 4824, respectively, whereas animals in the DMAb group tended to demonstrate the largest differences, with respective measures of 0.015 ± 0.006 (-51% vs. VEH; $p \leq 0.001$), 22.48 ± 5.61 μm (-34% vs. VEH; $p \leq 0.001$), 276.43 ± 44.87 μm (+13% vs. VEH; $p \leq 0.001$) , and 20473 ± 5568 (-17% vs. VEH; $p = 0.024$). Differences between VEH and the other antiresorptive groups were also observed, as reported in Table 2.

Finally, samples from animals treated with antiresorptives had greater apparent density ($p = 0.01$), dry density ($p = 0.010$), and ash density ($p = 0.003$), but not ash fraction ($p = 0.174$) compared with VEH. Dry density and ash density were greater in the DMAb group vs VEH, with respective measures of 1812.66 ± 285.90 kg/m^3 (+6.7%; $p = 0.03$) and 1279.27 ± 227.06 kg/m^3 (+8.65%; $p = 0.03$) for DMAb vs 1699.16 ± 167.77 kg/m^3 and 1177.40 ± 144.08 kg/m^3 in VEH. Animals in the VEH-DMAb group also demonstrated greater ash density than VEH, with a measure of 1279.69 ± 166.20 kg/m^3 (+8.68%; $p = 0.018$). We also observed differences in apparent density, where VEH-DMAb and ALN groups demonstrated greater density than VEH. These treatment groups demonstrated respective measures of 1913.77 ± 184.98 kg/m^3 (+5.87%; $p=0.005$) and 1929.48 ± 204.53 kg/m^3 (+6.75%; $p = 0.003$), compared to 1807.55 ± 198.24 kg/m^3 in the VEH group. Results from select mechanical, μCT, and density measures are shown in Figure 4.

4.0 Discussion

This study assessed differences in the fatigue life of cortical bone from mature ovariectomized NHPs after receiving 12 months of potent antiresorptive agents. Fatigue life was greater in animals treated with antiresorptive vs VEH, with statistically significant differences for the ALN, ALN-DMAB, and DMAb groups. Microarchitecture, measured via μCT, was different in all treatment groups vs VEH. Finally, apparent, dry, and ash density were greater in animals treated with antiresorptives, though no differences in ash fraction were detected. In summary, we detected no detrimental effects of antiresorptive agents that could explain the observed association between AFF and prolonged antiresorptive use [13]. In contrast, these findings suggest that 12 months of antiresorptive treatment has a protective effect against mechanical fatigue fractures, which may explain how these drugs help prevent insufficiency and/or fragility fracture in humans [6,7,11,12].

Two previously published animal studies [28,29] explored the effect of antiresorptive treatment on *in-vitro* measurement of bone fatigue life, with results that differ somewhat from our findings. Brock et al [29] assessed fatigue life using a diet-induced sheep model of osteoporosis, and reported no differences in fatigue life or modulus loss of femoral cortical beams after 12 months of therapy with the potent bisphosphonate zoledronic acid (ZOL) compared with VEH controls (n = 6 animals/group). However, the same article also reported that 12-months ALN was associated with lower fatigue life and greater modulus loss, but these results were derived from single cortical beams harvested from 2 ALN-treated sheep and 3 VEH-treated controls. As demonstrated in Figure 2, specimen-to-specimen variability in fatigue life can span several orders of magnitude and we believe that it is difficult to draw a strong conclusion from so few samples. Another study involving mechanically loaded rib bone from

gonad intact beagles found that 3-years treatment with ALN was associated with reduced fatigue life,[28] though this reported reduction was driven by lower initial modulus and there was no difference thereafter in loss of modulus between ALN and vehicle controls. In contrast, the current study shows higher initial modulus with ALN versus vehicle, and our results corroborate the lack of difference in loss of modulus with ALN versus vehicle thereafter. The investigators in the canine study also made the *a priori* decision (prior to unblinding) to exclude samples that failed quickly, before reaching the secondary phase of fatigue damage[41]. It is possible that these samples represent important sites of local structural weakness, where failure would likely initiate during whole bone loading; a follow-up report showed that inclusion of these samples influences the interpretation of their findings[42]. Our current study is the first to quantify fatigue life after antiresorptive use in a non-human primate model of postmenopausal osteoporosis. We believe these analyses, which were from a GLP-compliant study, provide important new insights into the effects of antiresorptive treatment on fatigue life in postmenopausal women with osteoporosis.

The differences in fatigue life detected here are consistent with our supporting measurements of mechanical properties, microarchitecture, and density. Similar to previous studies of ALN and DMAb on bone microarchitecture[3,43,44], all antiresorptive treatments demonstrated reduced porosity and smaller pore diameters that have been previously associated with improved fatigue life[37,45]. In the 12-month DMAb group, we were also able to detect greater dry and ash density, resulting in increased initial modulus and energy dissipation; this finding is consistent with the well-established relationships between porosity, density, and stiffness of bone [46,47]. We did not detect differences in ash fraction, suggesting that density differences were driven by differences in porosity rather than tissue composition. Follow-up analyses were also unable to detect treatment group differences in density-modulus relationships,

further supporting this hypothesis. Finally, it was somewhat surprising that apparent density was greater than VEH in the VEH-DMAb and ALN groups but not DMAb. We speculate that this measure may be sensitive to errors from PBS trapped in the pore space after hydration. Indeed, both VEH-DMAb and ALN groups had slightly larger (though not statistically significant) mean porosity and pore diameter compared to DMAb.

Considered in aggregate, our measurements of mechanical properties, microarchitecture and density suggest the mechanism by which these drugs influenced fatigue life of bone. In general, antiresorptive therapy reduced bone porosity and/or improved density. As a result, samples from antiresorptive treated animals tended to have a higher modulus than those from VEH treated animals, i.e., these samples experienced less strain under the applied load. Noting the well-established relationship between strain magnitude and fatigue life [48,49], this explains how/why samples from antiresorptive treated animals survived more cycles than VEH. Supporting our interpretation of the link between action of the drug, modulus, and fatigue life, we note that the effects of treatment could no longer be identified if comparing cycles to failure against a *modulus-normalized* stress (Figure S1, Online Supplemental Material).

If mirrored in humans, greater fatigue life after antiresorptive treatment may be a mechanism by which these drugs reduce fractures. Spontaneous insufficiency fractures are relatively common among elderly postmenopausal women[50] and can occur in different bones throughout the body[51]. These fractures are associated with repetitive normal loading of severely weakened bone, i.e., mechanical fatigue. Similarly, though fragility fractures of long bone are almost always associated with minor trauma such as a fall [52,53], it has been speculated that mechanical degradation from repetitive loading may influence fracture risk[54]. Though it is unclear precisely what percentage of clinical fracture cases have mechanical fatigue as an

underlying factor, improvement to bone fatigue life may be a mechanism by which these drugs reduce fracture rates in postmenopausal women[6,7,11,12].

Across all measures investigated in this study, i.e., fatigue life, mechanical properties, bone microarchitecture, or bone density measurements, we found either beneficial differences or no statistically significant differences vs VEH in ovariectomized NHPs treated for 12 months with DMAb, ALN, or DMAb after ALN. These parameters tended to be higher in proportion to the degree and duration of osteoclast inhibition, with the 12-month DMAb group showing the greatest improvements and the VEH-ALN group showing the smallest improvements. Though we cannot confirm if this trend would continue over longer treatment durations, our findings after 12 months of treatment do not support the hypothesis that osteoclast inhibition weakens bone or reduces its fatigue resistance.

Strengths of this study in comparison with previous nonclinical evaluations of *in-vitro* fatigue properties after antiresorptive therapy include the clinical relevance of aged ovariectomized NHPs, the GLP compliance of the original study, and the relatively robust sample size. Previously reported serum bone turnover markers and histomorphometry data from this study indicate profound reductions in systemic, trabecular, and intracortical bone remodeling with ALN and DMAb, providing a robust test of the hypothesis that remodeling inhibition does not impair bone fatigue properties[26]; in particular, the DMAb-treated NHPs received ~150-fold more DMAb per kg per year than do patients with osteoporosis, which led to near-total ablation of osteoclasts. Thus, these doses were likely sufficient to reveal any potential detrimental changes associated with suppressed remodeling.

This study also has a few important limitations. First, we quantified fatigue life in un-notched specimens; this allowed us to observe the consequences of the interrelated processes of

crack initiation and growth in a manner that we believe is highly relevant for clinical interpretation. Future studies may choose to introduce a flaw of known geometry into the specimens, which would allow for analysis using a linear-elastic fracture mechanics paradigm to quantify additional measures like fracture toughness and energy release rate. Next, animals received drug for a maximum of 12 months, which may reflect ~2-to-2.5 years of remodeling cycles in humans[55,56]. In humans, risk of AFF in the first year is low and steadily rises over time[57]. Future studies with longer treatment durations may be justified. These NHPs were essentially middle-aged, and older animals may have shown different results. Also, though AFF occurs in the femur in humans, this analysis was limited to humeral bone. Femur bones were previously used for histomorphometry[34] and destructive analyses [26] and were not available for this study. Though we cannot confirm that these results would be replicated at the femur, we note that the humerus of cynomolgus monkeys also experiences substantial loading, including compressive forces from quadrupedal locomotion and tensile forces from grasping, climbing, and swinging. While not equivalent to a fatigue testing protocol, monotonic loading of the femur in our previous study did not detect detrimental differences in stiffness and strength[26]. Moreover, this study used samples from the midshaft and proximal 1/3 of the humerus, which may be a reasonable analog for AFF sites in humans. Our study relied on *in-vitro* fatigue loading, and thus does not model potentially important interactions between antiresorptive therapy and 'in-service' microdamage and repair that may occur *in-vivo* over long durations. Finally, we recognize that AFF is a rare phenomenon [58] with potential relationships to unique biomechanical[59,60] and/or biological traits [61,62] that cannot be modeled in animals.

In light of the current results, it may be noteworthy that a recent clinical study[63] found higher AFF risk in individuals treated with the cathepsin K inhibitor odanacatib, a drug that

causes lesser inhibition of bone resorption than DMAb. This suggests that alternative hypotheses for the etiological link between antiresorptive use and AFF beyond the effects of osteoclast inhibition may be warranted. For example, reduced hip fracture risk with odanacatib, ALN, or DMAb may allow a subset of patients to continue loading femurs that otherwise would have experienced typical fragility fractures of the hip, and this continued loading could lead to the later development of fatigue-related failure in subtrochanteric and diaphyseal regions that generally show lesser structural and BMD improvements from drug, compared with the proximal femur (i.e., "hip survival bias")[64].

5.0 Conclusions

In this study we analyzed cortical bone from mature ovariectomized NHPs treated with antiresorptives for 12 months. We detected greater fatigue life in bone from animals in the ALN, ALN-DMAb and DMAb groups vs. VEH, and these differences were well explained by μCT measures of bone microarchitecture. All treatment groups demonstrated reduced porosity, smaller pore diameters, and lower number of canals vs VEH. We also detected differences in bone density, where 12-month DMAb demonstrated greater dry and ash density compared to VEH. Overall, we did not detect any detrimental differences that could indicate a mechanistic link between treatment and AFF in humans. In contrast, beneficial differences in fatigue life, microarchitecture, and bone density suggests a protective effect against insufficiency and fragility fractures, consistent with reduced fracture rates observed in humans following antiresorptive therapy[6,7,11,12].

6.0 Acknowledgements

This work was funded by an investigator-initiated grant from Amgen Inc. We would like to thank Wei Liu and Alexandra Olsen for their assistance with μCT image acquisition, as well as Jake Ruschkowski and Vincent Wu for assistance with image analysis. We would also like to thank Andy Pohl for assistance with the statistical methodology.

7.0 Disclosures

WBE has received research support and speaker fees from Amgen. SKB has received research support from Amgen. PJK is a former Amgen employee and has served as a contractor and consultant for Amgen. ITH, LLL, and AS have no disclosures.

8.0 Author Contributions

ITH: Investigation, methodology, software, formal analysis, writing – original draft preparation, writing – reviewing and editing. LLL: Investigation, methodology, software, writing – reviewing and editing. AS: Investigation, methodology, software, writing – reviewing and editing. PJK: Conceptualization (supporting), writing – reviewing and editing. SKB: Conceptualization (supporting), funding acquisition, resources, writing – reviewing and editing. WBE: Conceptualization (lead), funding acquisition, resources, supervision, writing – reviewing and editing. WBE takes responsibility for integrity of the data analysis.

9.0 Data availability

The data that support the findings of this study are available from the corresponding author upon reasonable request.

8.0 References

1. Kanis J a. Diagnosis of osteoporosis and assessment of fracture risk. Lancet [Internet]. 2002 Jun 1;359(9321):1929–36. Available from: http://www.ncbi.nlm.nih.gov/pubmed/12057569

2. Khosla S, Shane E. A crisis in the treatment of osteoporosis. J. Bone Miner. Res. 2016;31(8):1485–7.

3. Seeman E, Delmas PD, Hanley DA, Sellmeyer D, Cheung AM, Shane E, Kearns A, Thomas T, Boyd SK, Boutroy S, Bogado C, Majumdar S, Fan M, Libanati C, Zanchetta J. Microarchitectural deterioration of cortical and trabecular bone: differing effects of denosumab and alendronate. J. Bone Miner. Res. [Internet]. 2010 Aug;25(8):1886–94. Available from: https://onlinelibrary.wiley.com/doi/10.1002/jbmr.81

4. Burghardt AJ, Kazakia GJ, Sode M, De Papp AE, Link TM, Majumdar S. A longitudinal HR-pQCT study of alendronate treatment in postmenopausal women with low bone density: Relations among density, cortical and trabecular microarchitecture, biomechanics, and bone turnover. J. Bone Miner. Res. 2010;25(12):2558–71.

5. McClung MR, Lewiecki EM, Cohen SB, Bolognese MA, Woodson GC, Moffett AH, Peacock M, Miller PD, Lederman SN, Chesnut CH, Lain D, Kivitz AJ, Holloway DL, Zhang C, Peterson MC, Bekker PJ. Denosumab in postmenopausal women with low bone mineral density: Commentary. Obstet. Gynecol. Surv. 2006;61(6):384–6.

6. Liberman UA, Weiss SR, Bröll J, Minne HW, Quan H, Bell NH, Rodriguez-Portales J, Downs RW, Dequeker J, Favus M, Seeman E, Recker RR, Capizzi T, Santora AC, Lombardi A, Shah R V., Hirsch LJ, Karpf DB. Effect of oral alendronate on bone mineral density and the incidence of fractures in postmenopausal osteoporosis. N. Engl. J. Med. 1995;333(22):1437–44.

7. Pols HAPP, Felsenberg D, Hanley DA, Štepán J, Muñoz-Torres M, Wilkin TJ, Qin-Sheng G, Galich AM, Vandormael K, Yates AJ, Stych B, Group for the FITS. Multinational, placebo-controlled, randomized trial of the effects of alendronate on bone density and fracture risk in postmenopausal women with low bone mass: Results of the FOSIT study. Osteoporos. Int. [Internet]. 1999;9(5):461–8. Available from: https://doi.org/10.1007/PL00004171

8. Ferrari S, Libanati C, Lin CJF, Brown JP, Cosman F, Czerwiński E, de Gregório LH, Malouf-Sierra J, Reginster JY, Wang A, Wagman RB, Lewiecki EM. Relationship Between Bone Mineral Density T-Score and Nonvertebral Fracture Risk Over 10 Years of

Denosumab Treatment. J. Bone Miner. Res. 2019;34(6):1033–40.

9. Imai K, Ohnishi I, Matsumoto T, Yamamoto S, Nakamura K. Assessment of vertebral fracture risk and therapeutic effects of alendronate in postmenopausal women using a quantitative computed tomography-based nonlinear finite element method. Osteoporos. Int. 2009;20(5):801–10.

10. Zysset P, Pahr D, Engelke K, Genant HK, McClung MR, Kendler DL, Recknor C, Kinzl M, Schwiedrzik J, Museyko O, Wang A, Libanati C. Comparison of proximal femur and vertebral body strength improvements in the FREEDOM trial using an alternative finite element methodology. Bone [Internet]. Elsevier Inc.; 2015;81:122–30. Available from: http://dx.doi.org/10.1016/j.bone.2015.06.025

11. Nakamura T, Matsumoto T, Sugimoto T, Hosoi T, Miki T, Gorai I, Yoshikawa H, Tanaka Y, Tanaka S, Sone T, Nakano T, Ito M, Matsui S, Yoneda T, Takami H, Watanabe K, Osakabe T, Shiraki M, Fukunaga M. Clinical trials express: Fracture risk reduction with denosumab in Japanese postmenopausal women and men with osteoporosis: Denosumab Fracture Intervention Randomized Placebo Controlled Trial (DIRECT). J. Clin. Endocrinol. Metab. 2014;99(7):2599–607.

12. McCloskey E V., Johansson H, Oden A, Austin M, Siris E, Wang A, Lewiecki EM, Lorenc R, Libanati C, Kanis JA. Denosumab reduces the risk of osteoporotic fractures in postmenopausal women, particularly in those with moderate to high fracture risk as assessed with FRAX. J. Bone Miner. Res. 2012;27(7):1480–6.

13. Shane E, Burr D, Abrahamsen B, Adler RA, Brown TD, Cheung AM, Cosman F, Curtis JR, Dell R, Dempster DW, Ebeling PR, Einhorn TA, Genant HK, Geusens P, Klaushofer K, Lane JM, McKiernan F, McKinney R, Ng A, Nieves J, O'Keefe R, Papapoulos S, Howe T Sen, Van Der Meulen MCH, Weinstein RS, Whyte MP. Atypical subtrochanteric and diaphyseal femoral fractures: Second report of a task force of the American society for bone and mineral research. J. Bone Miner. Res. 2014;29(1):1–23.

14. Ural A. Biomechanical mechanisms of atypical femoral fracture. J. Mech. Behav. Biomed. Mater. [Internet]. Elsevier Ltd; 2021;124(July):104803. Available from: https://doi.org/10.1016/j.jmbbm.2021.104803

15. Allen MR, Gineyts E, Leeming DJ. Bisphosphonates alter trabecular bone collagen cross-linking and isomerization in beagle dog vertebra. Osteoporos. Int. 2008;19:329–37.

16. Acevedo C, Bale H, Gludovatz B, Wat A, Tang SY, Wang M, Busse B, Zimmermann EA, Schaible E, Allen MR, Burr DB, Ritchie RO. Alendronate treatment alters bone tissues at multiple structural levels in healthy canine cortical bone. Bone [Internet]. Elsevier B.V.; 2015;81:352–63. Available from: http://dx.doi.org/10.1016/j.bone.2015.08.002

17. Gourion-arsiquaud S, Allen MR, Burr DB, Vashishth D, Tang SY, Boskey AL. Bisphosphonate treatment modifies canine bone mineral and matrix properties and their heterogeneity. Bone. 2010;46(3):666–72.

18. Donnelly E, Meredith DS, Nguyen JT, Gladnick BP, Rebolledo BJ, Shaffer AD, Lorich DG, Joseph M, Lane JM, Boskey AL. Reduced cortical bone compositional heterogeneity with bisphosphonate treatment in postmenopausal women with intertrochanteric and

subtrochanteric fractures. J. Bone Miner. Res. 2015;27(3):672–8.

19. Allen MR, Iwata K, Phipps R, Burr DB. Alterations in canine vertebral bone turnover , microdamage accumulation , and biomechanical properties following 1-year treatment with clinical treatment doses of risedronate or alendronate. Bone. 2006;39:872–9.

20. Yamagami Y, Mashiba T, Iwata K, Tanaka M, Nozaki K, Yamamoto T. Effects of minodronic acid and alendronate on bone remodeling, microdamage accumulation, degree of mineralization and bone mechanical properties in ovariectomized cynomolgus monkeys. Bone. 2013;54(1):1–7.

21. Edwards WB, Loundagin L, Haider I. Fatigue Life Variation in Secondary Osteonal Bone is Primarily Determined by Vascular Canal Diameter Rather Than Generalized Porosity. ASMBR Annu. Meet. Orlando; 2019.

22. Burr DB. Fifty years of bisphosphonates: What are their mechanical effects on bone? Bone. 2020;138(June).

23. Allen MR, Reinwald S, Burr DB. Alendronate reduces bone toughness of ribs without significantly increasing microdamage accumulation in dogs following 3 years of daily treatment. Calcif. Tissue Int. 2008 May 8;82(5):354–60.

24. Burr DB, Liu Z, Allen MR. Duration-dependent effects of clinically relevant oral alendronate doses on cortical bone toughness in beagle dogs. Bone. 2015;71:58–62.

25. Lloyd AA, Gludovatz B, Riedel C, Luengo EA, Saiyed R, Marty E, Lorich DG, Lane JM, Ritchie RO, Busse B, Donnelly E. Atypical fracture with long-term bisphosphonate therapy is associated with altered cortical composition and reduced fracture resistance. Proc. Natl. Acad. Sci. U. S. A. 2017;114(33):8722–7.

26. Kostenuik PJ, Smith SY, Samadfam R, Jolette J, Zhou L, Ominsky MS. Effects of denosumab, alendronate, or denosumab following alendronate on bone turnover, calcium homeostasis, bone mass and bone strength in ovariectomized cynomolgus monkeys. J. Bone Miner. Res. 2015;30(4):657–69.

27. Karim L, Kwaczala A, Vashishth D, Judex S. Dose-dependent effects of pharmaceutical treatments on bone matrix properties in ovariectomized rats. Bone Reports [Internet]. Elsevier Inc.; 2021;15:101137. Available from: https://doi.org/10.1016/j.bonr.2021.101137

28. Bajaj D, Geissler JR, Allen MR, Burr DB, Fritton JC. The resistance of cortical bone tissue to failure under cyclic loading is reduced with alendronate. Bone [Internet]. Elsevier Inc.; 2014;64:57–64. Available from: http://dx.doi.org/10.1016/j.bone.2014.03.045

29. Brock GR, Chen JT, Ingraffea AR, MacLeay J, Pluhar GE, Boskey AL, van der Meulen MCH. The effect of osteoporosis treatments on fatigue properties of cortical bone tissue. Bone Reports. 2015;2:8–13.

30. Brown JP, Prince RL, Deal C, Recker RR, Kiel DP, De Gregorio LH, Hadji P, Hofbauer LC, Álvaro-Gracia JM, Wang H, Austin M, Wagman RB, Newmark R, Libanati C, San Martin J, Bone HG. Comparison of the effect of denosumab and alendronate on BMD and biochemical markers of bone turnover in postmenopausal women with low bone mass: A

randomized, blinded, phase 3 trial. J. Bone Miner. Res. 2009;24(1):153–61.

31. Burr DB. Estimated intracortical bone turnover in the femur of growing macaques: Implications for their use as models in skeletal pathology. Anat. Rec. 1992;232(2):180–9.

32. Jerome CP, Peterson PE. Nonhuman primate models in skeletal research. Bone. 2001;29(1):1–6.

33. Ominsky MS, Stouch B, Schroeder J, Pyrah I, Stolina M, Smith SY, Kostenuik PJ. Denosumab, a fully human RANKL antibody, reduced bone turnover markers and increased trabecular and cortical bone mass, density, and strength in ovariectomized cynomolgus monkeys. Bone [Internet]. Elsevier Inc.; 2011;49(2):162–73. Available from: http://dx.doi.org/10.1016/j.bone.2011.04.001

34. Kostenuik PJ, Smith SY, Jolette J, Schroeder J, Pyrah I, Ominsky MS. Decreased bone remodeling and porosity are associated with improved bone strength in ovariectomized cynomolgus monkeys treated with denosumab, a fully human RANKL antibody. Bone [Internet]. Elsevier Inc.; 2011;49(2):151–61. Available from: http://dx.doi.org/10.1016/j.bone.2011.03.769

35. Koeppen VA, Schilcher J, Aspenberg P. Dichotomous location of 160 atypical femoral fractures. Acta Orthop. 2013;84(6):561–4.

36. Taylor D. Fatigue of bone and bones: An analysis based on stressed volume. J. Orthop. Res. 1998;16(2):163–9.

37. Loundagin LL, Edwards WB. Stressed volume around vascular canals explains compressive fatigue life variation of secondary osteonal bone but not plexiform bone. J. Mech. Behav. Biomed. Mater. [Internet]. Elsevier Ltd; 2020;111(June):104002. Available from: https://doi.org/10.1016/j.jmbbm.2020.104002

38. Doube M, Kłosowski MM, Arganda-Carreras I, Cordelières FP, Dougherty RP, Jackson JS, Schmid B, Hutchinson JR, Shefelbine SJ. BoneJ: Free and extensible bone image analysis in ImageJ. Bone [Internet]. 2010 Dec;47(6):1076–9. Available from: https://linkinghub.elsevier.com/retrieve/pii/S8756328210014419

39. Tony S. K. Predicting the compressive mechanical behavior of bone. J. Biomech. [Internet]. 1994;27(9):1159–68. Available from: http://www.sciencedirect.com/science/article/pii/0021929094900566%5Cnhttp://pdn.sciencedirect.com/science?_ob=MiamiImageURL&_cid=271132&_user=499885&_pii=0021929094900566&_check=y&_origin=article&_zone=toolbar&_coverDate=30-Sep-1994&view=c&originContentFa

40. Loundagin LL, Pohl AJ, Edwards WB. Stressed volume estimated by finite element analysis predicts the fatigue life of human cortical bone: The role of vascular canals as stress concentrators. Bone [Internet]. Elsevier; 2021;143(September 2020):115647. Available from: https://doi.org/10.1016/j.bone.2020.115647

41. Bajaj D, Geissler JR, Allen MR, Burr DB, Fritton JC. Response to Courtney et al. Bone [Internet]. Elsevier Inc.; 2016;89:77–9. Available from: http://dx.doi.org/10.1016/j.bone.2015.03.007

42. Courtney A, Corrigan CF, Steffey D. Letter to the Editor regarding Bajaj D, et al., The resistance of cortical bone tissue to failure under cyclic loading is reduced with alendronate, Bone 2014;64:57–64. Bone [Internet]. Elsevier Inc.; 2016;89:80–1. Available from: http://dx.doi.org/10.1016/j.bone.2015.03.008

43. Roschger P, Rinnerthaler S, Yates J, Rodan GA, Fratzl P, Klaushofer K. Alendronate increases degree and uniformity of mineralization in cancellous bone and decreases the porosity in cortical bone of osteoporotic women. Bone. 2001;29(2):185–91.

44. Lespessailles E, Hambli R, Ferrari S. Osteoporosis drug effects on cortical and trabecular bone microstructure: a review of HR-pQCT analyses. Bonekey Rep. [Internet]. Nature Publishing Group; 2016;5(June):1–8. Available from: http://dx.doi.org/10.1038/bonekey.2016.59

45. Loundagin LL, Haider IT, Cooper DML, Edwards WB. Association between intracortical microarchitecture and the compressive fatigue life of human bone: A pilot study. Bone Reports [Internet]. Elsevier; 2020;12(February):100254. Available from: https://doi.org/10.1016/j.bonr.2020.100254

46. Wachter NJ, Krischak GD, Mentzel M, Sarkar MR, Ebinger T, Kinzl L, Claes L, Augat P. Correlation of bone mineral density with strength and microstructural parameters of cortical bone in vitro. Bone [Internet]. Elsevier Science Inc.; 2002;31(1):90–5. Available from: http://dx.doi.org/10.1016/S8756-3282(02)00779-2

47. Bayraktar HH, Morgan EF, Niebur GL, Morris GE, Wong EK, Keaveny TM. Comparison of the elastic and yield properties of human femoral trabecular and cortical bone tissue. J. Biomech. [Internet]. 2004 Jan [cited 2011 Aug 9];37(1):27–35. Available from: http://linkinghub.elsevier.com/retrieve/pii/S0021929003002574

48. Carter DR, Caler WE, Spengler DM, Frankel VH. Fatigue behavior of adult cortical bone: the influence of mean strain and strain range. Acta Orthop. 1981;52(5):481–90.

49. Zioupos P, Currey JD, Casinos A. Tensile Fatigue in Bone: Are Cycles-, or Time to Failure, or Both, Important? J. Theor. Biol. [Internet]. 2001 Jun;210(3):389–99. Available from: http://linkinghub.elsevier.com/retrieve/pii/S0022519301923161

50. Brennan M, O'Shea PM, O'Keeffe ST, Mulkerrin EC. Spontaneous Insufficiency Fractures. J. Nutr. Heal. Aging. 2019;23(8):758–60.

51. Soubrier M, Dubost JJ, Boisgard S, Sauvezie B, Gaillard P, Luc Michel J, Ristori JM. Insufficiency fracture. A survey of 60 cases and review of the literature. Jt. Bone Spine. 2003;70(3):209–18.

52. Nevitt MC, Cummings SR. Type of Fall and Risk of Hip and Wrist Fractures: The Study of Osteoporotic Fractures. J. Am. Geriatr. Soc. [Internet]. 1993 Nov;41(11):1226–34. Available from: https://onlinelibrary.wiley.com/doi/10.1111/j.1532-5415.1993.tb07307.x

53. Anderson DE, Burkhart K, Alemi MM, Bouxsein ML. Biomechanics of hip and vertebral fractures [Internet]. Marcus Feldman's Osteoporos. INC; 2020. Available from: http://dx.doi.org/10.1016/B978-0-12-813073-5.00016-2

54. Hernandez CJ, van der Meulen MCH. Understanding Bone Strength Is Not Enough. J.

Bone Miner. Res. 2017;32(6):1157–62.

55. Burr DB, Hirano T, Turner CH, Hotchkiss C, Brommage R, Hock JM. Intermittently administered human parathyroid hormone(1-34) treatment increases intracortical bone turnover and porosity without reducing bone strength in the humerus of ovariectomized cynomolgus monkeys. J. Bone Miner. Res. 2001;16(1):157–65.

56. Recker RR, Delmas PD, Halse J, Reid IR, Boonen S, Garcia-Hernandez PA, Supronik J, Lewiecki EM, Ochoa L, Miller P, Hu H, Mesenbrink P, Hartl F, Gasser J, Eriksen EF. Effects of intravenous zoledronic acid once yearly on bone remodeling and bone structure. J. Bone Miner. Res. 2008;23(1):6–16.

57. Schilcher J, Koeppen V, Aspenberg P, Michaëlsson K. Risk of atypical femoral fracture during and after bisphosphonate use. Acta Orthop. 2015;86(1):100–7.

58. Mahjoub Z, Jean S, Leclerc JT, Brown JP, Boulet D, Pelet S, Grondin C, Dumont J, Belzile ÉL, Michou L. Incidence and characteristics of atypical femoral fractures: clinical and geometrical data. J. Bone Miner. Res. 2016;31(4):767–76.

59. Oh Y, Wakabayashi Y, Kurosa Y, Fujita K, Okawa A. Potential pathogenic mechanism for stress fractures of the bowed femoral shaft in the elderly: Mechanical analysis by the CT-based finite element method. Injury. 2014;45(11):1764–71.

60. Haider ITIT, Schneider P, Michalski A, Edwards WBB. Influence of geometry on proximal femoral shaft strains: Implications for atypical femoral fracture. Bone. Elsevier Inc.; 2018;110:295–303.

61. Dhanekula ND, Crouch G, Byth K, Lau SL, Kim A, Graham E, Ellis A, Clifton-Bligh RJ, Girgis CM. Asian Ethnicity and Femoral Geometry in Atypical Femur Fractures: Independent or Interdependent Risk Factors? JBMR Plus. 2022;6(4):1–8.

62. Oh Y, Yamamoto K, Hashimoto J, Fujita K, Yoshii T, Fukushima K, Kurosa Y, Wakabayashi Y, Kitagawa M, Okawa A. Biological activity is not suppressed in mid-shaft stress fracture of the bowed femoral shaft unlike in "typical" atypical subtrochanteric femoral fracture: A proposed theory of atypical femoral fracture subtypes. Bone [Internet]. Elsevier; 2020;137(February):115453. Available from: https://doi.org/10.1016/j.bone.2020.115453

63. Papapoulos S, Bone H, Cosman F, Dempster DW, McClung MR, Nakamura T, Restrepo JFM, Bouxsein ML, Cohn D, de Papp A, Massaad R, Santora A. Incidence of Hip and Subtrochanteric/Femoral Shaft Fractures in Postmenopausal Women With Osteoporosis in the Phase 3 Long-Term Odanacatib Fracture Trial. J. Bone Miner. Res. 2021;36(7):1225–34.

64. Silverman S, Kupperman E, Bukata S. Bisphosphonate-related atypical femoral fracture: Managing a rare but serious complication. Cleve. Clin. J. Med. 2018;85(11):885–93.

Table 1 Mechanical fatigue testing results.

		VEH N=48;12/Load		VEH-DMAb N=48;12/Load		ALN* N=48;12/Load		ALN-DMAb* N=48;12/Load		DMAb* N=48;12/Load	
	Load Level [MPa]	Median	IQR	Median	IQR	Median	IQR	Median	IQR	Median	IQR
Fatigue Life [cycles-to-failure]	80	162089	172726	463239	644963	622245	746236	639833	691024	429648	611635
	100	59897	85437	79867	144645	78260	156757	195193	382322	91304	305734
	120	18094	33060	11606	22821	12449	19279	32901	45690	246463	243864
	140	1987	10593	3633	30819	9850	13648	10493	16796	14495	49299

*Group demonstrated $p < 0.05$ vs. VEH.

Table 2 Summary of mechanical, μCT, and density measures. All measures were evaluated with a Kruskal-Wallis test, the p-value of which is also shown. Note that 2 samples could not be recovered after fatigue testing and were not available for imaging or density measures.

		VEH (N=48)		VEH-DMAb (N=47)		ALN (N=47)		ALN-DMAb (N=48)		DMAb (N=48)		p
		Median	IQR	Median	IQR	Median	IQR	Median	IQR	Median	IQR	
Mechanical Properties	N	48		48		48		48		48		
	Initial Modulus [GPa]	16.94	6.60	18.16	6.45	19.00	5.74	18.77	5.24	**19.82*,·,†**	6.22	<0.001
	Modulus Loss	0.39	0.28	0.33	0.30	0.33	0.25	0.38	0.26	0.32	0.30	0.340
	Energy Dissipation [J/mm3]	1.53	3.16	2.05	5.94	1.83	7.44	2.46	7.96	**4.40***	7.95	0.018
μCT	N	48		47		47		48		48		
	Porosity	0.031	0.032	**0.019***	0.008	**0.018***	0.017	**0.013*,·,†**	0.011	**0.015***	0.006	<0.001
	Mean Pore diameter [μm]	34.20	34.50	**25.23***	10.62	**25.16***	18.62	**22.36***	7.83	**22.48***	5.61	<0.001
	Max Pore diameter [μm]	76.82	82.65	**49.11***	36.94	**60.74**	62.78	**45.30*,·,α**	15.78	**42.43*,·,α**	15.25	<0.001
	Mean Pore spacing [μm]	242.08	56.10	**275.85***	99.97	**285.34***	59.05	**297.76***	89.04	**276.43***	44.87	<0.001
	Number of Canals	24764	4824	**19013***	8113	**19911***	7295	**17399***	7643	**20473***	5568	<0.001
Density	N	48		47		47		48		48		
	Apparent Density [kg/m^3]	1807.55	198.24	**1913.77***	184.98	**1929.48***	196.90	1843.33	242.16	1895.95	326.66	0.002
	Dry Density [kg/m^3]	1699.16	167.77	1786.43	244.07	1772.41	163.90	1765.88	114.05	**1812.66***	285.90	0.009
	Ash Density [kg/m^3]	1177.40	144.08	**1279.69***	166.20	1211.98	167.08	1241.58	123.01	**1279.27***	227.06	0.002
	Ash Fraction	0.69	0.07	0.70	0.08	0.68	0.06	0.70	0.05	0.69	0.07	0.174

*Indicates $p \leq 0.05$ vs VEH; †Indicates $p \leq 0.05$ vs. VEH-DMAb; ·$^{\alpha}$Indicates $p \leq$ vs. ALN